Proc. Symp. Soil Behavior and Soft Ground Construction, in honor of Charles C. Ladd - October 2001, MIT

Soil Behavior at the Microscale: Particle Forces

J. Carlos Santamarina[1]

Abstract

Soils are particulate materials. Therefore, the behavior of soils is determined by the forces particles experience. These include forces due to boundary loads (transmitted through the skeleton), particle-level forces (gravitational, buoyant, and hydrodynamic), and contact level forces (capillary, electrical and cementation-reactive). The relative balance between these forces permits identifying various domains of soil behavior. Furthermore, the evolution of particle forces helps explain phenomena related to unsaturation, differences between drained and undrained strength under various loading modes (including the effect of plasticity), sampling disturbance, and fines migration during seepage. Generally accepted concepts gain new clarity when re-interpreted at the level of particle forces.

Introduction

The limitations with continuum theories for the analysis of soil behavior were recognized early in the twentieth century. Terzaghi wrote "… Coulomb… purposely ignored the fact that sand consists of individual grains, and … dealt with the sand as if it were a homogeneous mass with certain mechanical properties. Coulomb's idea proved very useful as a working hypothesis for the solution of one special problem of the earth-pressure theory, but it developed into an obstacle against further progress as soon as its hypothetical character came to be forgotten by Coulomb's successors. The way out of the difficulty lies in dropping the old fundamental principles and starting again from the elementary fact that sand consists of individual grains" (Terzaghi 1920 - includes references to previous researchers).

The fundamental understanding of soil behavior begins by recognizing the particulate nature of soils and its immediate implications: the interplay between particle characteristics (e.g., size, shape, mineralogy), inter-particle arrangement and interconnected porosity, inherently non-linear non-elastic contact phenomena, and

[1] Professor, School of Civil and Environmental Engineering, Georgia Institute of Technology, Atlanta, GA 30332. E-mail: carlos@ce.gatech.edu.

particle forces. While all these parameters are interrelated, the focus of this manuscript is on particle forces, their relative importance, and the re-interpretation of soil phenomena relevant to engineering applications with emphasis on processes studied by Prof. C. Ladd. Finally, the microscale analysis of forces leads to a re-interpretation of the effective stress principle and previously suggested modifications.

Particle Forces

Particle forces in soils were considered in the seminal paper by Ingles (1962), and later reviewed in Mitchell (1993) and Santamarina et al. (2001-a). Particle forces are classified herein in relation to the location of the generation mechanism:

- *Forces due to applied boundary stresses*: they are transmitted along granular chains that form within the soil skeleton. Capillary effects at high degree of saturation prior to air-entry fall under this category.
- *Particle-level forces*: includes particle weight, buoyancy and hydrodynamic forces. A particle can experience these forces even in the absence of a soil skeleton.
- *Contact-level forces*: includes capillary forces at low degree of saturation, electrical forces, and the cementation-reactive force. The first two can cause strains in the soil mass even at constant boundary loads. Conversely, the cementation-reactive force opposes skeletal deformation.

Mass-related magnetic forces (not relevant in most soils) and contact-level hydrodynamic squirt-flow type forces (that develop during dynamic excitation) are not considered in this review. The emphasis in this section is on recent developments in the understanding of particle forces, and includes simple, order-of-magnitude expressions to estimate these forces for the case of spherical particles.

Skeletal Forces (related to applied boundary stresses)

Early analyses based on spherical particles and regular packings (Deresiewicz 1973), photoelastic models (Durelli and Wu 1984), and the more recent developments in numerical micro-mechanics pioneered by Cundall (Cundall and Strack 1979) have provided unique insight into the distribution and evolution of inter-particle skeletal forces in soils.

Both normal N and tangential T forces develop at contacts when an effective stress σ' is applied at the boundary[2]. The normal force N at a contact is related to the applied state of effective stress σ' and the particle diameter d. The first order approximation $N= d^2\sigma'$ is appropriate for a simple cubic packing of equal size spheres. For a random packing of spheres, the mean normal contact force $\underline{N}$ is related to the void ratio e through some empirical or semi-empirical correction functions, rendering expressions such as (for $0.4<e<1$)

$$\underline{N} = \sigma' d^2 \left[\frac{\pi(1+e)^2}{12} \right] \qquad (1)$$

[2] For convenience, the more common equivalent continuum concept of "stress" is herein used to refer to the distributed force applied at the boundary.

The boundary stress is not supported uniformly by the skeletal forces N and Weibull or exponential distributions apply (Dantu 1968; Gherbi et al. 1993; Jaeger et al. 1996). Further insight is gained from photoelastic studies such as those shown in Figure 1:

- Chains of particles form columnar structures that resist the applied boundary stress (Drescher and de Josselin de Jong 1972; Oda et al. 1985). These chains resemble a fractal-type structure. The smallest scale of chains is a few particle diameters in size. Particles that form part of these chains are loaded in the direction of the applied principal stress.
- Particles that are not part of the main chains play the secondary yet very important role of preventing the buckling of the main chains. Hence, the main forces acting on these particles are transverse to the main chains (Radjai et al. 1998 - see Figure 1-a).
- There are many particles that sit within the granular medium and do not carry skeletal load. These are "movable" particles and, if smaller than the pore throats, may migrate when proper fluid flow conditions develop in the medium.
- When large pores are present, force chains arch around the pores. These arches tend to collapse during shear (see Figure 1-b).
- The stability of the columns is related to the direction of particle movement during loading, so that reversing the direction of loading promotes instability. Load history dependency is manifested even at small deformations as shown in Figure 1c (Duffy and Mindlin 1957): the stiffness contributed by the contact shear resistance would be lost if the loading direction is reversed.

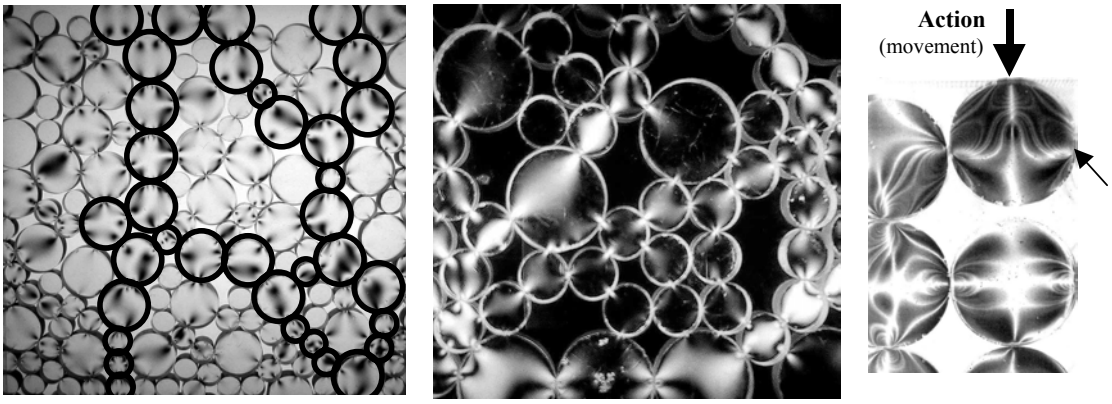

Figure 1: Skeletal force distribution – Photoelastic disks. (a) Random packing and force chains - different force directions along principal chains and in secondary particles (b) arches around large pores - precarious stability around pores. (c) Resistance mobilized during loading - contribution of shear stiffness (Courtesy of J. Valdes, M. Guimaraes, and M. Aloufi).

While the increase in mean stress promotes volume reduction and a higher coordination number (contacts) between particles, the increase in deviatoric load causes internal anisotropy in contact distribution. Inter-particle coordination and its anisotropy restrict the possible axis of rotation eventually leading to rotational arrest or frustration (Figure 2). In general, the probability for rotational frustration increases

with increasing coordination, i.e., with decreasing void ratio (the dense system shown on the right is frustrated for any rotation). Therefore, rotational frustration is overcome by either frictional slippage at contacts or by fabric changes that lead to fewer contacts among particles, i.e., decreasing coordination number which is often associated with local dilation. In fact, the higher interparticle friction, the lower the extent of frictional slippage at contacts, and the lower the coordination number that develops during shear (see Thornton 2000). While these concepts are illustrated with monosize spherical particles, rotational frustration is affected by the relative size among neighboring particles, by the ability to attain high densities in soils with high coefficient of uniformity, and by particle shape (sphericity, angularity and roughness).

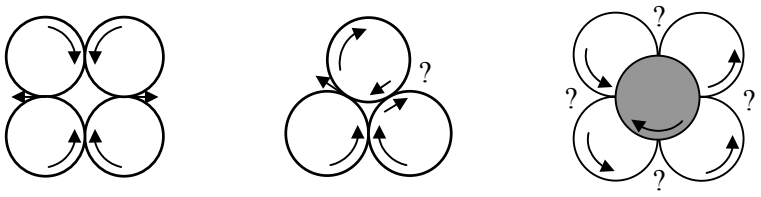

Figure 2. Rotational frustration. The lower the void ratio, the higher the number of contacts per particle and the higher the probability of rotational frustration.

These observations gain further relevance in the context of 3D micro-mechanical simulations of axial compression AC (b=0) and axial extension AE (b=1), where $b=(\sigma_2-\sigma_3)/(\sigma_1-\sigma_3)$. The distribution of contacts and average normal and shear contact forces in a given direction θ, herein denoted as $\underline{N}(\theta)$ and $\underline{T}(\theta)$, are depicted in Figure 3 (Chantawarangul 1993; see also Rothenburg and Bathurst 1989, and Thornton 2000). The following observations can be made:

- Contact normals during anisotropic loading become preferentially oriented in the direction of the main principal stress σ_1, in agreement with observations made above (see also Oda 1972).
- The main reduction in inter-particle contacts takes place in the direction of the minor principal stress: σ_2 and σ_3 directions in AC, and σ_3 direction in AE. This situation allows for more degrees of freedom for particle rotation and for chain buckling in AC (even when the total coordination number at failure is about the same in both cases).
- Such volume-average microscale response provides insight into the observed effective peak friction angle (macroscale - numerical results presented in the lower frame of Figure 3): higher friction angle is mobilized in AE than in AC. Furthermore, the lack of particle displacement in the direction of plane strain hinders rearrangement and causes an even higher peak friction angle in plane strain loading. The critical state friction angle obtained in numerical simulations follows a similar trend, but with less pronounced differences.
- Results by Chantawarangul (1993 - not presented here) also show that early volume contraction before the peak strength, is more pronounced in AE than in AC tests – relevant to undrained strength.

3D Distribution of:	(a) Isotropic confinement	At peak deviatoric load	
		(b) Axial Compression b=0	(c) Axial Extension b=1
Contact normals			
Average Normal Contact Force $\underline{N}(\theta)$			
Average Shear Contact Force $\underline{T}(\theta)$ (magnified x5)			
Friction angle	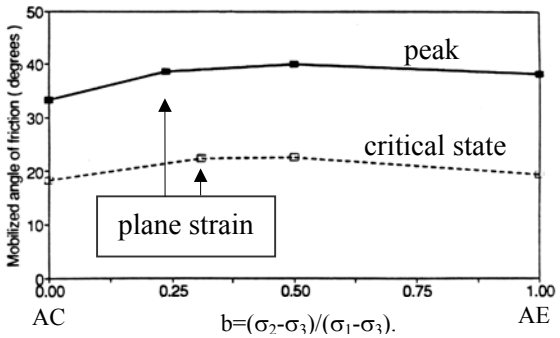		

Figure 3. Numerical simulation: Evolution of inter-particle contacts and average normal and shear contact forces during axial compression and axial extension loading. Variation in friction angle with the intermediate stress σ_2. Figure compiled from Chantawarangul (1993).

The evolution of anisotropy in contact normals and in contact forces $\underline{N}(\theta)$ and $\underline{T}(\theta)$ reflects the soil response to the anisotropic state of stress that is applied at the boundaries. Ultimately, *the shear strength of a soil is the balance between two competing trends: the reduction in coordination to minimize frictional resistance by freeing particle rotation, and the increase in coordination following the buckling of particle chains.* Therefore, the shear strength of a soil reflects the restrictions to particle motion due to either mutual frustration or boundary conditions.

Gravitational Force: Weight and Buoyancy (Particle-Level)

Newton's fourth law specifies the attraction force between two masses m_1 and m_2 at a distance r: $F_G=Gm_1m_2/r^2$, where $G=6.673x10^{-11}$ $N\cdot m^2/kg^2$. This force causes tides as the moon interacts with oceans, and gives rise to the weight of soil grains on the earth (e.g., m_1 is the mass of the earth and m_2 is the mass of a soil grain); for a spherical particle of diameter d is,

$$W = \frac{1}{6}\pi G_s \gamma_w d^3 \qquad \textit{Weight of a sphere} \qquad (2)$$

where G_s is the specific gravity of the mineral that makes the particle and γ_w is the unit weight of water. The gravitational attraction F_G between two grains is much smaller than the weight of grains (about 10^{12} times smaller for millimetric particles).

Hydrostatic fluid pressure results from the weight of the fluid above the point under consideration. When a particle is submerged in water (or any other fluid), the water pressure is normal to the particle surface. The integral of the fluid pressure acting on the particle renders the buoyancy force. This force does not change, regardless of the submerged depth because the difference between the water pressure acting at the bottom and at the top of the particle remains the same, $\Delta u=\gamma_w d$ (rigid particles). In Archimedes' words, the buoyant force is equal to the weight of fluid the particle displaces, regardless of depth. For completeness,

$$U = Vol \cdot \gamma_w = \frac{1}{6}\pi \gamma_w d^3 \qquad \textit{Buoyant force} \qquad (3)$$

The effective weight of a submerged particle becomes W-U.

A related experiment considers the case of two soil grains press together using a clamp, and submerged into a pond. The particles experience not only the same buoyant force but also the same inter-particle contact force due to the clamp at all depths (Figure 4). Hence, *the local pore fluid pressure around a particle does not alter the effective inter-particle skeletal force*.

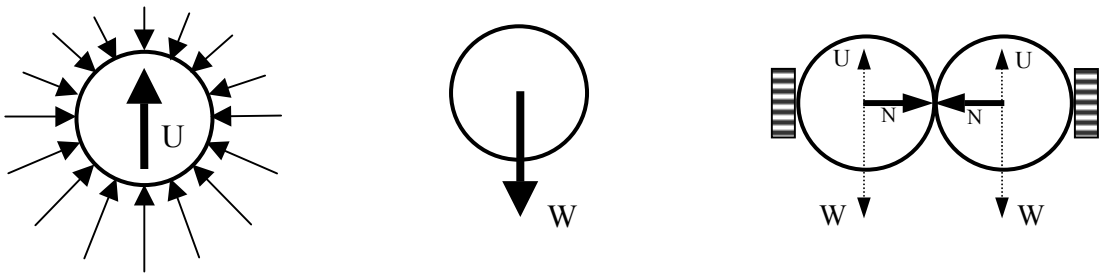

Figure 4 Hydrostatic fluid pressure, buoyant force U, weight W, and inter-particle skeletal forces N.

Hydrodynamic Force (Particle-Level)

The pore fluid moving along the interconnected pore network in the soil exerts viscous drag forces and forces resulting from velocity gradients (null average in straight macro-flow). Consider the pore fluid moving with velocity v relative to a particle of diameter d. The magnitude of the viscous drag force F_{drag} is proportional to the viscosity of the fluid μ, as predicted by Stoke's equation (applies to low Reynolds numbers - Graf 1984; Bear 1972):

$$F_{drag} = 3\pi\mu v d \tag{4}$$

where the viscosity of water at 20°C is $\mu \cong 1$ centiPoise=0.001 N·s/m^2. The velocity of fluid moving through the pores in a soil is related to the hydraulic gradient i, the hydraulic conductivity k, and the porosity n of the soil, v= ki/n. Combining this relation with Equation 4 permits estimating the drag force experienced by a potentially movable particle sitting on a pore wall. Viscous drag also acts on the particles that form the skeleton, and together with the velocity gradient forces alters the effective stress acting on the soil (often referred to as the seepage force).

Capillary Force - Mixed Fluid Phase (Boundary to Contact-Level)

A molecule in a fluid experiences van der Waals attraction to neighboring molecules. As these forces act in all directions, they tend to cancel. However, this is not the case for water molecules at the surface of the fluid: these molecules feel an effective pull-in resultant force normal to the fluid surface. At the macroscale, this effect resembles a membrane that tries to shrink, creating a surface tension T_s which characterizes the interface (T_s=0.0727 N/m for water-air at room temperature). Because this membrane tries to shrink, the fluid inside drops has positive pressure. This pore fluid pressure is computed using Laplace's equation,

$$u = T_s\left(\frac{1}{r_1} + \frac{1}{r_2}\right) \tag{5}$$

where r_1 and r_2 are the curvature radii of the air-water interface. For a spherical drop, r_1=r_2.

On the other hand, water tends to wet and hydrate hydrophilic mineral surfaces. When a saturated soil mass begins to dry, the gradually shrinking volume of water pulls the membrane in, while the membrane attempts to cling to the mineral surfaces around pore throats. Therefore, suction develops inside the pore fluid. The membrane tension is transmitted onto the skeleton in terms of effective stress, as in a triaxial specimen surrounded by a thin membrane and subjected to vacuum, hence, the force acting on particles at this stage develops at the *boundary*. As desiccation progresses, air gradually invades the specimen. If the fluid phase remains continuous, the medium is in the funicular regime. The average interparticle force $F_{cap}=\pi d^2 u/4$, is

computed by invoking Equation 5. Radii r_1 and r_2 are related to the diameter d_{pore} of the largest pore at the air-water interface where the front is currently receding (the effective value for d_{pore} is about the diameter d of the particles surrounding the pore),

$$F_{cap} = \pi \frac{d^2}{d_{pore}} T_s \qquad \textit{Funicular regime} \qquad (6)$$

At very low moisture content, disconnected fluid remains in the form of menisci at inter-particle contacts; this is the pendular regime. Figure 5 shows a sequence of microphotographs that capture the drying of water in the menisci between two spherical particles. As menisci dry, the negative pressure increases, and the cross section decreases. The contact-level capillary force computed from Laplace's equation at very low moisture content is (asymptotic solution for $w\% \rightarrow 0$; the value of F_{cap} is limited by water cavitation),

$$F_{cap} = \pi d T_s \qquad \textit{Pendular regime (contact-level)} \qquad (7)$$

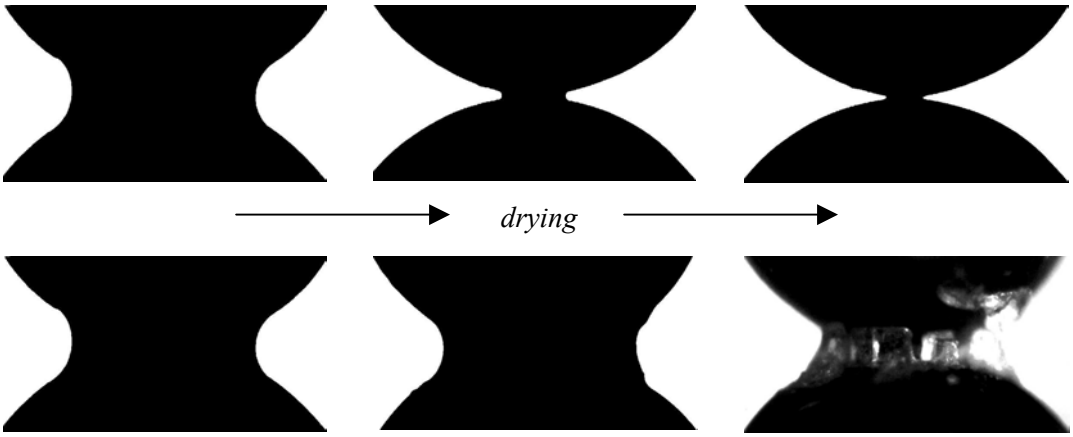

Figure 5. Evolution of unsaturation – Pendular regime. The lower spherical glass bead (d= 2mm) is being held by the meniscus. Top sequence: de-ionized water. Lower sequence: water has salt in solution, salts eventually precipitate rendering inter-particle cementation (Gathered with D. Fratta).

Note that capillary forces in clays can be very high even at high degree of saturation, because d_{pore} is very small (Equation 6; in the presence of soluble salts and double layers, the total suction combines matric suction and osmotic suction - see Fredlund and Rahardjo 1993).

As the air-water interface gradually recedes during drying, it displaces first along the largest pores it encounters, then, the smaller pores are evacuated. Therefore, the negative pore fluid pressure increases as drying continues, and the evolution of inter-particle forces reflects the pore size distribution of the soil, as seen at the receding front. Pore size distribution is related to grain size distribution, thus, the suction-moisture plot resembles the grain size distribution of the soil (as observed in

Öberg 1997). Because of the stiffening effect of suction on soils, there is also a strong parallelism between the shear wave velocity vs. moisture plot and the grain size distribution plot (Cho and Santamarina, 2001 – continuously drying tests without remixing).

Electrical Forces (Contact-Level)

Can uncemented remolded soils exhibit cohesion? This can be tested by preparing a mud ball, submerging it in water to cancel capillary effects, and observing if the soil crumbles and reaches the angle of repose. This experiment must be carefully conducted to avoid seepage forces, entrapped air, diffusion and osmotic effects. Consider the following simple procedure to avoid these difficulties: a few grams of soil are mixed with some selected solution inside a test tube (diameter much larger than the particle size), the system is allowed to homogenize for 24 hr, a vacuum is applied to extract all the air while shaking the test tube, and the sediment is consolidated by subjecting the test tube to a high g-field in a centrifuge. Finally, the top is sealed with wax to avoid entrapping any air, and the tube is inverted. This is a very simple tension test. Kaolinite specimens prepared following these guidelines have been kept upside down for more than two years and no detachment has been observed (Figure 6). Clearly, the electrical attraction between particles is sufficient to support their buoyant weight.

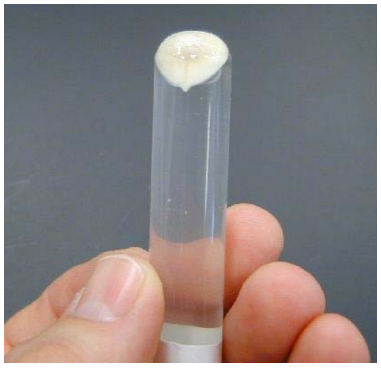

Figure 6. Electrical attraction forces are greater than the particle buoyant weight in fine soils (experimental details in the text – gathered with Y.H. Wang).

While the study of contact-level electrical forces started more than a century ago, molecular dynamic simulations and atomic force microscopy studies in the last 20 years have provided unprecedented information. The essence of all phenomena involved is the interplay between geometric compatibility, thermal agitation and Coulomb's electrical force. As a result, various repulsion and attraction forces develop, and the balance between these forces varies with inter-particle distance, rendering a highly non-linear force-distance relation. A brief review follows.

When the inter-particle distance exceeds ~30-40 Å, the response is well described disregarding the molecular nature of water molecules and the atomic nature of charges. Both, van der Waals attraction and electrical repulsion must be considered

(DLVO theory). The van der Waals attraction between two spherical particles of equal diameter d is (Israelachvili 1992),

$$Att = \frac{A_h}{24t^2} d \qquad \textit{van der Waals attraction} \qquad (8)$$

where t is the separation between particles, and the Hamaker constant for silica-water-silica is $A_h=0.64*10^{-20}$J. Repulsion results from thermal agitation and kinetic effects (also referred to as osmotic pressure or entropic confinement). The repulsion force between two spherical particles of diameter d is (derived after Israelachvili 1992 – applies to low surface potential and inter-particle distance $t>\vartheta$)

$$\begin{aligned} Rep &= 32\pi RTc_o d\vartheta e^{-\frac{t}{\vartheta}} \\ &\approx 0.0024 d\sqrt{c_o}\ e^{-10^8 t\sqrt{c_o}} \end{aligned} \qquad \textit{Electrical repulsion force} \qquad (9)$$

where the gas constant R=8.314 J/(mol.K), T is temperature [°K], c_o is the ionic concentration of the pore fluid [mole/m^3], and the double layer thickness or Debye-Huckel length in units of [m] is equal to $\vartheta= 9.65\cdot10^{-9}(c_o)^{-0.5}$ for monovalent ions. The second simplified equation applies to monovalent ions, T=298°K, distance t in [m] and the force in [N].

At smaller distances, the ionic concentration between the particles exceeds the pore fluid concentration c_o, the osmotic pressure becomes independent of c_o and it is only a function of the particle surface charge density. In turn, the effective surface charge density and the surface potential gradually decrease as particles come closer together due to ion binding (Delville, 2001). In this range, the electrostatic attraction force may exceed the van der Waals attraction, particularly when di-valent and tri-valent ions are present. Di-valent and tri-valent ions such as Ca^{2+} and Al^{3+} are most effective at shielding the electric field generated by the particle (lowering the surface potential), and if they bind to the particle, they may even render the particle positively charged. High-valence ions also interact among themselves so their positions are correlated, causing an additional attraction force between particles. Because of these effects, the presence of di-valent and tri-valent ions hinders the swelling of clays; these effects are not taken into consideration in the DLVO theory, therefore, this theory applies best to mono-valent ions.

When the inter-particle distance is less than ~10-20Å, the discrete nature of ions and water molecules must be recognized (the size of a water molecule is ~2.8 Å). In this range, the behavior of the particle-fluid-particle system resembles two plates with marbles in between: the molecular structure tends to be crystal-like ordered, friction is understood within the framework of thin film lubrication (Bhushan et al. 1995; Landman et al. 1996; Persson 1998), the water-ion system is organized reflecting the counterions' affinity for water and the density profile oscillates (Skipper et al. 1991; Delville 1995), inter-particle forces vary cyclically with distance with a periodicity of about one molecular diameter ("hydration force" - experimental data first reported in Horn and Israelachvili 1981), swelling progresses by discrete jumps

("hydration swelling"), and ionic mobility and diffusion are reduced (Skipper, 2001). Finally, at very high applied load, mineral to mineral interaction could develop and interpenetration is opposed by Born repulsion at the atomic level.

This framework explains most colloidal phenomena, including coagulation and swelling as a function of ionic concentration, as well as the effect of changes in fluid permittivity (changes in Hamaker constant and ion hydration). Yet, the direct application of these concepts could be misleading. For example, the sedimentation volume observed in test tubes does not decrease monotonically with ionic concentration, but often starts increasing at high concentration (Figure 7): either the form of aggregation of individual particles changes (e.g., from face-to-face "domains" to edge-to-face), or already formed domains flocculate forming open edge-to-face flocculation (Emerson 1959; Bennett and Hulbert 1986). Similar trends can be found in mechanical properties such as viscosity vs. concentration (e.g., van Olphen 1991). The transition concentration depends on clay mineralogy and pH.

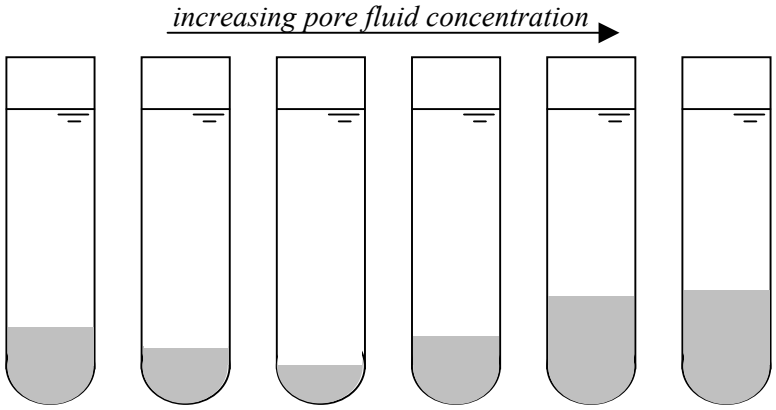

Figure 7. Electrical forces and fabric. The increase in ionic concentration above a characteristic value may render lower density fabrics (response varies with pH and mineralogy).

Cementation-reactive Force (Contact-Level)

There are many mechanisms leading to cementation. Figure 5 shows the evaporation of water in the meniscus between two particles and the precipitation of salt, forming crystals that bond the particles together. Some agents lithify the soil around particles and at contacts, while other processes change the initial physical-chemical structure (Mitchell 1993; Larsen and Chilingar 1979). Cementation is a natural consequence of aging and the ensuing diagenetic effects in soils. Most natural soils have some degree of inter-particle bonding (e.g., an ingenious device and data for London clay are presented in Bishop and Garga 1969).

Cementation is often accompanied by either shrinkage or swelling, and the ensuing changes in inter-particle skeletal forces. However, the most significant mechanical contribution of cementation is activated when strains are imposed onto the soil. To facilitate comparing this cementation-reactive force to other forces, the tensile force required to break the cement at a contact is computed herein. Consider a

homogeneous layer of cementing material of thickness t deposited all around particles of diameter d. The diameter of the cement across the contact is determined by the Pythagorean relation; for small cement thickness, $d^2_{cont}=4d\cdot t$. Then, for a cement with tensile strength σ_{ten}, the maximum tensile force that the contact may withstand is

$$T = \pi\, t\, d\, \sigma_{ten} \tag{10}$$

Even small amounts of cementation may produce significant changes in the behavior of soils if the confinement is relatively low.

Forces: Relative Relevance and Implications

The relative balance between particle forces gives rise to various regimes and phenomena in soils that affect geotechnical engineering practice. A few salient examples follow. Phenomena studied by Prof. C. Ladd or reported in two comprehensive reviews he co-authored are often invoked (Ladd et al. 1977; Jamiolkowski et al. 1985; Ladd 1991 Terzaghi Lecture).

Skeletal -vs- Contact-Level Forces

Skeletal, capillary, and van der Waals forces contribute to the normal compressive contact force (the contribution of particle weight is in the vertical downwards direction and may be compressive if sitting or tensile if the particle is hanging). Their relative contributions for different size spherical particles are depicted in Figure 8 (using previous equations; van der Waals attraction is computed for an inter-particle separation of 30 Å. The skeletal force is shown for σ'=10 kPa and σ'=1 MPa). These compressive forces mobilize the electrical repulsion forces and bring particles together until compression and repulsion are balanced. Changing the pore fluid can alter the inter-particle distance at equilibrium; the upper part of the figure shows the strain caused by changing the pore fluid from fresh-water to seawater concentrations (axis on the right - Equation 9 combined with Equations 1 and 8). The following observations can be made:

- Particle weight looses relevance with respect to capillary forces for particles smaller than d≈3mm (Point 1 in the figure), and with respect to van der Waals attraction for particles smaller than d≈30μm (Point 2 in the figure).
- Capillary forces can exceed the contribution of σ'=10 kPa confinement for particles smaller than d≈20μm (Point 3) and the contribution of σ'=1 MPa for d<0.2μm (Point 4).
- Judging by the strain level, chemical-mechanical coupling gains relevance for micron and sub-micron particles: the smaller the particles or the lower the effective confinement, the greater the effect of changes in pore fluid chemistry.
- Particles are considered "coarse" when skeletal forces due to boundary loads prevail. This is the case for particles larger than d≈20μm (Point 3).
- Particles are "fine" when contact-level capillary and electrical forces gain relevance. This is the case when particles are smaller than d≈1-10μm.

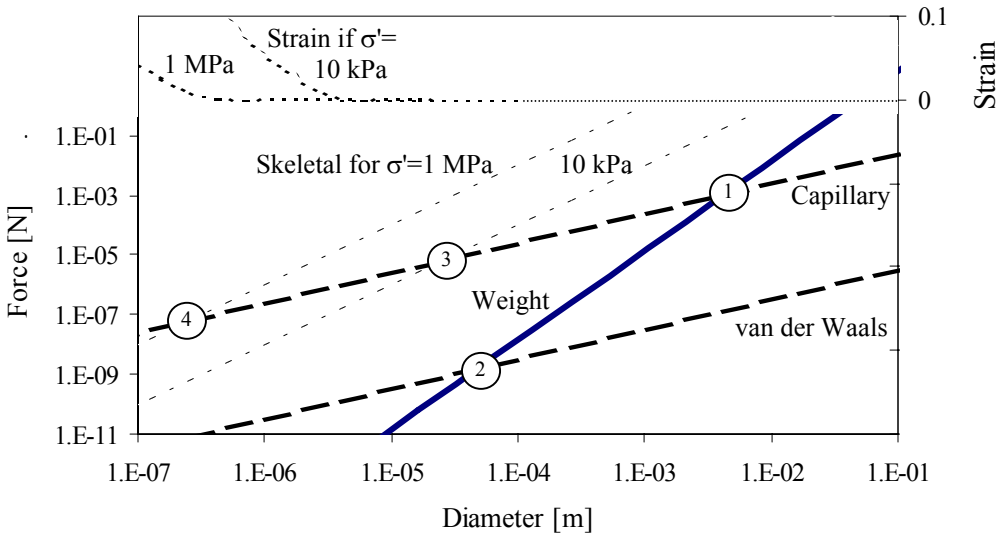

Figure 8. Skeletal vs. contact-level capillary and electrical forces. The upper part of the figure shows the strain (axis on right) caused by changing the pore fluid ionic concentration from fresh-water to seawater conditions. Note slopes: skeletal 2:1 (Equation 1), weight 3:1 (Equation 2), capillary and van der Waals 1:1 (Equations 6, 7 and 8).

The contribution of the van der Waals attraction force remains much smaller than the skeletal force under normal engineering conditions, even for very small particles. In the absence of cementation (or edge-to-face coordination), the classification of fine soils as "cohesive soils" is misleading and physically unjustified (two related views are presented in Santamarina 1997, and in Schofield 1998). Still, electrical forces determine fabric formation (Figure 7), which in turn affects soil behavior. A soil that has formed within a high ionic concentration fluid develops a characteristic fabric; if it is then leached with fresh water while confined, it may preserve the salient features of its fabric, yet, for a different inter-particle force condition. Therefore, it is not at its minimum energy configuration (as shown in Figure 7) and it is unstable. This is the case of sensitive marine clays.

The opposite case is equally important: when the soil fabric is already formed within a certain pore fluid, leaching a soil with a fluid with higher ionic concentration and/or valence produces a reduction in the inter-particle repulsion force (Equation 9), causing: a decrease in volume under a given effective stress condition, an increase in shear wave velocity, and an increase in hydraulic conductivity. Note that there are documented exceptions to these trends (an extensive compilation of experimental studies can be found in Santamarina et al. 2001-b). The response depends on the history of the test and whether stress or strain-controlled boundary conditions are imposed. Similar observations also apply to clay swelling (Ladd 1959).

Skeletal Forces -vs- Cementation - Sampling Effects

The stress-strain behavior, the strength and the volume change tendency of soils can be drastically affected by the degree of cementation (Clough et al. 1981; Lade

and Overton 1989; Airey and Fahey 1991; Reddy and Saxena 1993; Cuccovillo and Coop 1997). Two regions can be identified: the "cementation-controlled" region at low confinement, and the "stress-controlled" region at high confinement. In the cementation-controlled region, the small-strain shear stiffness can increase by an order of magnitude, the strength is cementation controlled, the buckling of chains is hindered (lower initial volume contraction), and the soil tends to brake in blocks (immediately after breaking, the inter block porosity is null, hence shear tends to cause high dilation, even if the cemented soil within the blocks has high void ratio).

The relative relevance of cementation and confinement can be identified by comparing the shear wave velocity in situ V_{So} with the velocity in a remolded specimen $V_{s\text{-}remold}$ that is subjected to the same state of stress. In general, one should suspect cementation if $V_{So} > V_{S\text{-}remold}$ (Note: creep and viscous effects also increase the shear wave velocity; these effects may be altered during sampling as well).

In most cases, natural cementation occurs when the soil is under confinement. When the soil is sampled, the applied confinement is removed, the center-to-center distance between particles increases, and the cement at contacts is put into tension. If the change in contact force $\Delta N=\Delta\sigma' d^2$ due to the stress reduction $\Delta\sigma'$ exceeds the tensile capacity of the cement at contacts (Equation 10), debonding occurs and the soil is permanently damaged or destructured. The cementation thickness can be related to the shear modulus of the soil G_s by considering a modified Hertzian formulation (Fernandez and Santamarina, 2001). Then, the following expression can be derived to predict the magnitude of stress reduction that can cause debonding σ'_{debond}:

$$\Delta\sigma' > \sigma'_{debond} = 1.9\sigma_{ten}\left(\frac{G_s}{G_g}\right)^2 \qquad \textit{condition for de-bonding} \qquad (11)$$

where σ_{ten} is the tensile strength of the bonding agent and G_g is the shear modulus of the mineral that makes the particles. The shear modulus of the soil G_s can be determined from the shear wave velocity V_{so} measured in situ as $G_s=\rho_s V_{so}^2$, where ρ_s is the mass density of the soil mass. The probability of debonding increases if the stress reduction $\Delta\sigma'$ approaches or exceeds the soil capacity $\Delta\sigma'_{debond}$. The upper bound for stress reduction is the in situ state of stress $\Delta\sigma'\approx\sigma_o'$ (details and data in Ladd and Lambe 1963). While G_g and σ_{ten} cannot be readily evaluated, this equation highlights the importance of the in situ shear wave velocity V_{so} in determining whether a soil will experience sampling effects due to stress reduction. Figure 9 summarizes these observations into four regions, and provides a framework for organizing available data and further studies on sampling effects (sampling disturbance is reviewed in Jamiolkowski et al. 1985). Note that it is premature to predict the potential impact of sampling on the bases of the in-situ shear wave velocity V_{So} alone.

De-bonding during sampling affects the behavior of both sands and clays, and it can cause important differences between the soil response measured in the laboratory

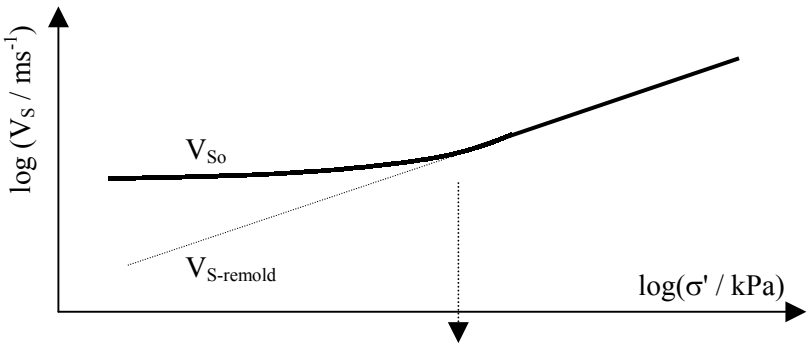

	Cement-controlled behavior $V_{So}>V_{S\text{-remold}}$	**Stress-controlled behavior** $V_{So}\approx V_{S\text{-remold}}$
No debonding $\Delta\sigma' < \Delta\sigma'_{debond}$	No sampling effect (sandstone at shallow depth)	No sampling effect (weakly cemented soil at depth)
Debonding $\Delta\sigma' > \Delta\sigma'_{debond}$.	stress reduction during sampling affects the measured properties	No sampling effect (soil debonds, but behavior is determined by σ')

Figure 9. Skeletal forces vs. cementation strength – Sampling and debonding.

and in the field (Tatsuoka and Shibuya 1992; Leroueil, 2001; data by Stokoe published in Stokoe and Santamarina 2000).

In line with the main emphasis of this manuscript, the preceding analysis was done in terms of contact forces and stress reduction. Alternatively, the analysis can be generalized in terms of strains (or particle-level deformation) and compared against the linear and degradation threshold strain of the soil. Stress reduction is the prevailing mechanism in block sampling; with other samplers, insertion and removal of the specimens cause additional stresses, pore pressure changes and volume changes in the soil that must also be taken into consideration.

Drag Force, Weight and Electrical Forces - Fines Migration

The potential for fines migration during seepage depends on the balance between the drag force, the weight of the particle and other resisting contact forces. Figure 10 shows the drag force for different pore flow velocities in comparison with the sum of the weight and the van der Waals attraction (computed for a possible Rep-Att minimum at 30 Å and at 100 Å inter-particle distances). Notice that:

- The migration of particles greater than about 100 μm is unlikely (the required pore flow velocity would render a turbulent regime).
- The migration of particles less than ~10 μm is determined by the electrical forces. In this case, changing the pore fluid chemistry can alter the force balance. For

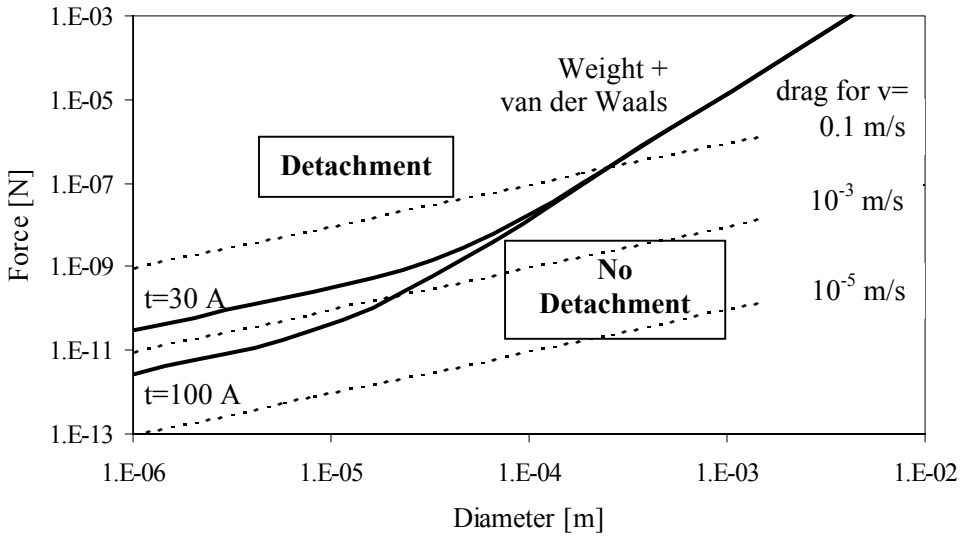

Figure 10. Drag vs. weight and net electrical attraction force.

example, a low concentration front may promote massive particle detachment allowing for particle migration.

- While individual small particles may not be detached, flocks of particles may.

For the conditions considered in the figure, a minimum pore flow velocity $v \approx 10^{-3}$ m/s is needed to cause detachment of any particle. Such pore flow velocity can be attained in sands or in coarse silts at high gradients. Therefore movable particles or "fines migration" is only relevant in the coarser formations and at high gradients, such as near a well.

Particles that are dragged may be flushed out of the soil or may form bridges at pore throats clogging the soil. Flushing and clogging depend on the relative size of the pore throats between skeleton-forming particles d_{large}, the size of the smaller migrating particles d_{small}, their ability to form bridges, and the volumetric concentration of fines in the permeant (Valdes 2002). In general, the required condition for flushing to occur is d_{large}/d_{small}>15-to-30. These microscale considerations provide insight into filter criteria. Whether flushing or clogging develops, the movement of the movable particles renders fluid flow non-linear, causing pressure jumps and changes in effective stress.

Skeletal Force Distribution: Effective Stress Strength (Friction Angle)

Micromechanical analyses and simulations show the relevance of particle coordination, rotational frustration and the buckling of chains on the ability of a soil to mobilize internal shear strength (Figures 1, 2 and 3). Such analyses predict that: (1) the friction angle is highest in plane strain, then in axial extension, and least in axial compression, (2) the difference in peak friction between plane strain and AC increases with inter-particle friction and density due to the enhanced rotational frustration, and (3) the difference among critical state friction angles determined at different b-values is smaller than among peak friction values. All these

micromechanical-based predictions are matched with experimental data gathered with sands (Figure 11-a and results in references such as Cornforth 1964; Bolton 1986; Schanz and Vermeer 1996). The evidence for any variation in critical state friction angle with b is less conclusive, yet minor differences may exist. Differences in friction angle in AE and AC are observed in clays as well, as shown in Figure 11.

The effect of the intermediate stress is not captured in Coulomb's failure criterion which predicts equal frictional resistance for all b-values, and it was first considered in the model by Lade and Duncan (1975).

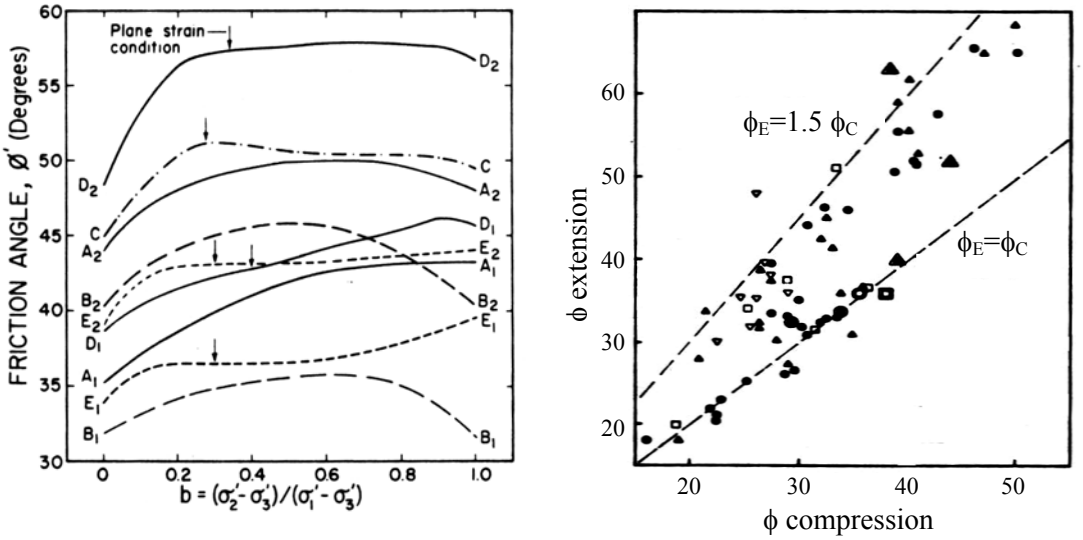

Figure 11. The effect of the intermediate stress on friction angle. (a) Sands - data from different authors compiled by Ladd et al. 1977 – Compare with Figure 3. (b) Clays: friction angle measured in AE b=0 and AC b=1 loading paths - from Mayne and Holtz (1985 - Most specimens are normally consolidated under K_o conditions).

Skeletal Force Distribution: Undrained Strength (D_r and PI effects)

Ladd (1967) disclosed differences in undrained shear strength measured in different loading paths. As the undrained strength is controlled by the generation of pore pressure, the following microscale mechanisms should be considered:

1. The buckling of particle chains and the consequent transfer of confinement onto the pore fluid pressure. Buckling vulnerability increases in soils that have been anisotropically consolidated (Figure 3), and when subsequent loading reverses the direction of deformation and the lateral stability of columnar chains is altered. Displacement reversal also faces lower skeleton stiffness (Figure 1c). As mentioned earlier, a higher tendency to early volume contraction in AE than AC is observed in micromechanical simulations.
2. Spatial variability in void ratio and the increased instability of chains around large pores (Figure 1b).

3. Cementation (even slight), long-range electrical forces in small particles, and menisci at particle contacts in a mixed fluid-phase condition (e.g., soils with oil-water mixtures) provide contact stability and hinder buckling.
4. Inherent fabric anisotropy and its effects on skeletal stability and compressibility.

It follows from the first observation that AE loading should be more damaging than AC loading. The supportive experimental evidence is overwhelming, in sands (Hanzawa 1980, Vaid and Sivathayalan 1996, Yoshimine et al. 1999, Robertson et al. 2000, Vaid and Sivathayalan, 2000), silts (Zdravkovic and Jardine 1997), and clays (Bjerrum 1972, Ladd et al. 1977, Mayne and Holtz 1985, Jamiolkowski et al. 1985). Differences between AC and lateral extension LE, or between AE and lateral compression LC are less conclusive (e.g., Campanella and Vaid 1972; Parry 1960). Figure 12 shows data for sands and clays.

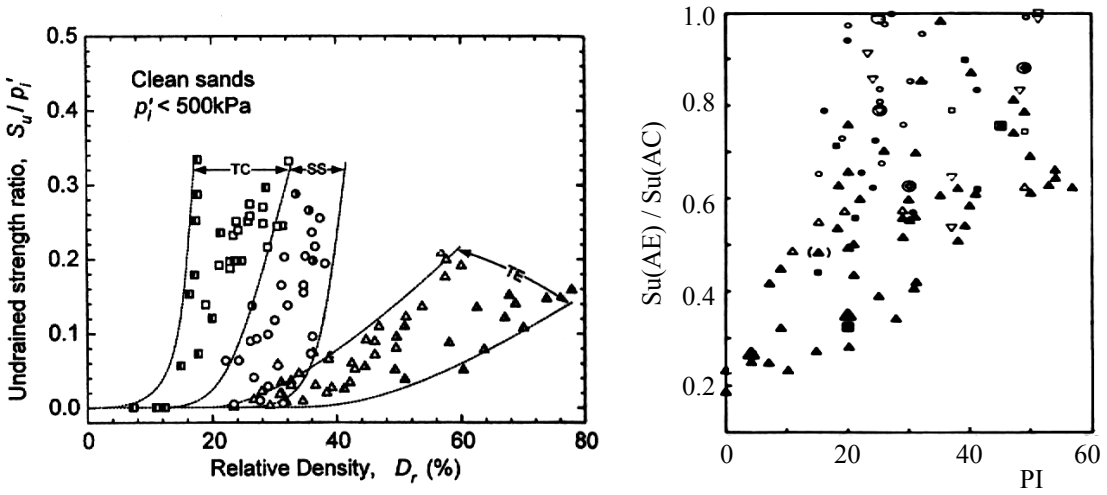

Figure 12. (a) Sands: comparison between undrained strength in triaxial axial compression TC, simple shear SS, and triaxial axial extension TE for various sands as a function of relative density (Yoshimine et al. 1999). (b) Clays: Undrained shear strength anisotropy Su(AE) / Su(AC) as a function of the plasticity of the clay; most specimens are normally consolidated under K_o conditions. Strength is defined at the maximum principal stress difference (Mayne and Holtz 1985).

Clearly, the collapse vulnerability of chains increases with decreasing relative density of sands, as particle coordination decreases (Figure 12-a). A related factor not captured in this figure is the effect of spatial variability of void ratio: arches around large pores are most vulnerable during shear (Figure 1b), hence, large pores tend to close first, as experimentally observed in soils (Sridharan et al. 1971; Delage and Lefebvre 1984). The spatial void ratio variability is related to specimen preparation methods (Castro 1969; Jang and Frost 1998). Hence, the undrained strength in soils is not only affected by the mean porosity, but by the pore size distribution as well (soil response for different specimen preparation methods is reviewed in Ishihara 1996).

The effect of plasticity in clays, shown in Figure 12-b, deserves special consideration. The typical role of electrical forces extends from about h=50 to 100 Å. Figure 13 compares a Hertzian-type analysis of the degradation threshold strain γ_{dt} applicable to coarse elastic particles, with an analysis applicable to small rigid particles where the threshold strain is calculated for a limiting thickness h that keeps particles "in touch". The corresponding relations are:

$$\gamma_{dt} = 1.3\left(\frac{\sigma'}{G_g}\right)^{2/3} \qquad \textit{Coarse grains} \qquad (12)$$

$$\gamma_{dt} = 1.2\frac{h}{d} \qquad \textit{Fine grains} \qquad (13)$$

where d is the particle diameter, G_g is the shear modulus of the mineral that makes the grains and σ' is the applied effective confining stress.

Figure 13. Contact forces and contact deformability - Degradation threshold strain. (a) Large particles: Hertzian deformation. (b) Small particles: electrical interaction.

The distance h for relevant inter-particle electrical interaction can be related to the thickness of the double layer ϑ. The value of h is in the range of 20 Å to 70 Å. The liquid limit and the plastic index of a soil are proportional to h and 1/d (Muhunthan 1991) therefore, Equation 13 confirms the link between PI and the degradation threshold strain observed by Vucetic and Dobry (1991). Then, the higher the plasticity of the clay, the higher the degradation threshold strain, the less vulnerable force chains are to buckling, and the lower the undrained strength anisotropy in axial extension vs. axial compression (Figure 12) The stabilizing effect of electrical forces can be readily confirmed by saturating soils specimens with non-polar fluids (S. Burns, personal communication).

Strength anisotropy data reflect the combined consequences of inherent fabric anisotropy and stress-induced anisotropy. Inherent fabric anisotropy results from either particle eccentricity and/or the biasing effects of deposition in a gravitational field. Its effect on undrained strength anisotropy can be explicitly studied by rotating the direction of the specimen an angle α with respect to the deposition direction (see data for sands and clays in Ladd et al. 1977; Jamiolkowski et al. 1985; Vaid and Sivathayalan 2000; for drained response in sand: Vaid and Sayao 1995). To facilitate

the visualization of depositional anisotropy effects, consider the extreme anisotropic packing of platy particles illustrated in the sketches on the left side of Figure 14: all contact normals and normal contact forces are in the vertical direction, all particle axes and contact shear forces are in the horizontal direction, and all pores are of equal size and geometry. Clearly, particle slenderness enhances contact and force anisotropy. The following responses are expected in the mind experiments proposed in the sketches:

- AC (b=0, α=0) causes minimum pore pressure generation.
- AE or LC (b=1, α=90) causes high initial pore pressure, followed by the development of kinematic constraints and possible dilatancy after "phase transformation".
- Simple shear SS (b>0, α=>0) may not only produce excess pore pressure but also a failure that is aligned with particle orientation so minimum dilatancy may be mobilized.

The structure sketched in Figure 14 could form during the slow deposition of large platy particles, such as mica platelets, so that gravity prevails over electrical forces. However, particles with slenderness as low as ~1.1/1.0 can confer large fabric anisotropy effects to the soil (Rothenburg 1993). This is the case not only in clays but also in most sands; data for Fraser River sand is presented in Figure 14[3].

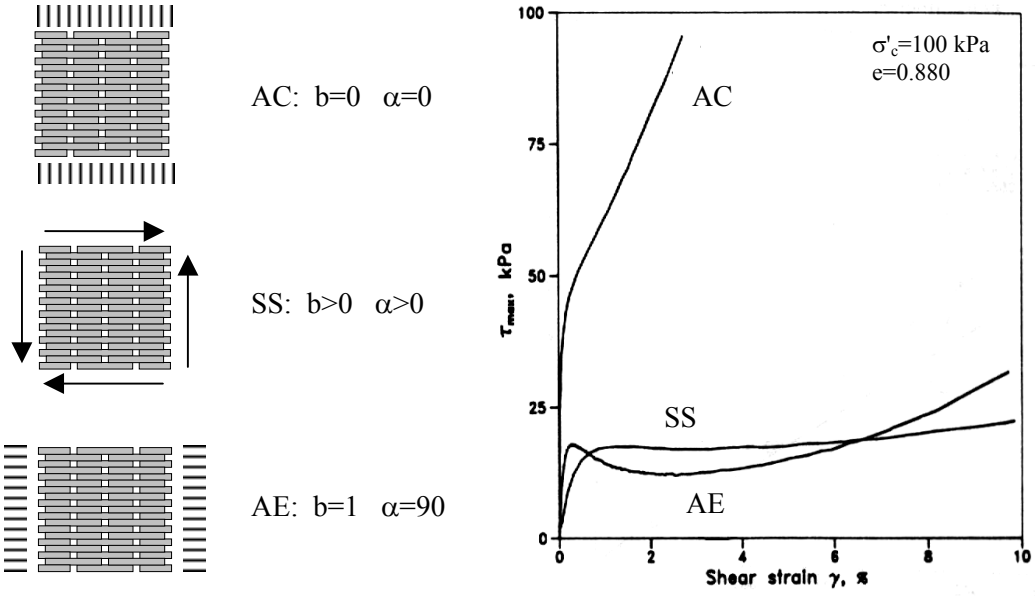

Figure 14. Inherent anisotropy effects on undrained strength. Left: conceptual models. Right: data for sands from Vaid and Sivathayalan (1996).

[3] Note: most numerical micromechanical simulations do not include gravity and depositional anisotropy (e.g., simulation in Figure 3). Slender particles accentuate the effects of stress induced anisotropy.

Spatial and Temporal Scales in Particle Forces

The variation in sedimentation volume with concentration shown in Figure 7 and the distribution of inter-particle skeletal forces forming particle chains shown in Figure 1 highlight the presence of multiple internal spatial scales in the medium. These scales add scale-dependent phenomena. For example, the distribution of skeletal forces (which reflects the interplay between chain buckling and rotational frustration) causes an uneven displacement field related to the mobilization of normal and shear forces at particle contacts and the threshold for frictional slippage, $T_{ult}=N\mu$. Individual particles move together by forming wedges that displace relative to each other along inter-wedge planes where the deformation localizes; eventually, the displacement becomes kinematically restricted, columns buckle, wedges break and new inter-wedge planes form. This behavior can be readily verified by assembling a 2D random packing of coins on a flat surface and enforcing the displacement of one boundary (Figure 15 – see Drescher and de Josselin de Jong 1972). Note that domains made of fine particles form conglomerates that can move in wedges as coarse grains; this observation can facilitate explaining the similarities between fine and coarse grained soil response, such as in Figure 11.

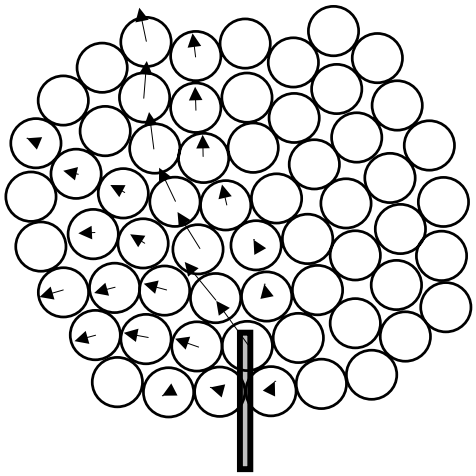

Vectors indicate the displacement of disks as the rod shown at the bottom is pushed into the assembly

Figure 15. Localization at the particle level – Wedges. At the particle level, the deformation in granular media is inherently uneven. (Test procedure: pennies on a scanner).

At larger scales, the localization of deformation leads to the development of shear bands, where the buckling of particle columns tends to concentrate (Oda and Kazama 1998). Therefore, the localization of deformation is an inherent characteristic of particulate materials, and it has been observed in dense-dilative soils under drained loading and under undrained loading (if cavitation is reached), loose-contractive soils under undrained loading, lightly cemented soils, unsaturated soils, soils with platy or rod-like particles, and heterogeneous soils (e.g., Vardoulakis 1996; Finno et al. 1997;

Saada et al. 1999; Mokni and Desrues 1998; Cho 2001). The development of global localization affects the interpretation of laboratory data, including results presented in Figures 11 and 12: the strain level at the formation of a shear band is a function of b (Lanier et al.1997, Wang and Lade, 2001), peak strength becomes specimen-size dependent as a function of soil rigidity and brittleness due to the associated "progressive failure", the measured global void ratio at large strain deviates from the critical state void ratio (Desrues et al. 1996), and the interpretation of the critical state friction angle is affected by the inclination of the shear band.

Particle forces also experience time-effects. The following examples apply to the different particle forces addressed above:

- *Normal and shear skeletal forces - Creep*. Two mechanisms are identified: First, material creep within particles near the contact (Kuhn and Mitchell 1993; Rothenburg 1993). Second, frictional slip; in this case the time scale at the particle level is determined by the inertial effects and the stress drop σ, $t=\sqrt{(d^2\rho/\sigma)}$. Supporting evidence is obtained with acoustic emission measurements.
- *Pore fluid pressure - Transient*. The most common time dependent effect in soils is the diffusion of excess pore pressure. While the boundary-level effect is considered in standard practice (this is the typical case in Terzaghi's consolidation), pressure differences also develop at the level of pores, for example, in dual porosity soils. The time scale for the dissipation of these local gradients or pressure diffusion is related to the internal length scale L_{int} and the internal coefficient of consolidation $c_{v\text{-}int}$ which depends on the skeletal stiffness and permeability, $t=L_{int}^2/c_{v\text{-}int}$.
- *Capillary force.* When an unsaturated soil is subjected to shear, equilibrium in the water-air potentials is not regained immediately. When the water phase is continuous (funicular regime), the time scale is determined by the hydraulic conductivity of the medium and tends to be short. When the water phase is discontinuous and remains only at contacts (pendular regime), pressure homogenization occurs through the vapor pressure and is very slow. Evidence gathered with shear wave velocity is presented in Cho and Santamarina (2001).
- *Electrical forces*. Forcing a relative displacement between particles alters the statistical equilibrium position of counterions around particles, hence, the inter-particle forces. The time for ionic stabilization can be estimated using the ionic diffusion coefficient D, as $t=d^2/D$. Time varying changes in electrical conductivity after remolding a soil specimen was observed by Rinaldi (1998). Additionally, viscous effects take place during the transient.
- *Cementation*. Diagenesis is clearly time-dependent and depends on the rate of chemical reactions and diffusion.

Particle-level time scales and macro-scale time scales in soils can be very different. The steady-state distribution of forces within a particulate medium presumes that equilibrium has been reached at all particles. When equilibrium is not attained at a given particle, the particle displaces and alters the equilibrium of its neighbors. Therefore, while it would appear that the particle-level time scales listed above tend to be short in general, their manifestation at the level of the soil can extend for a long period of time due to the large number of particles that are recursively involved, even if only the particles along main chains are considered.

Time-dependency in particle forces is related to macroscale phenomena observed in soils such as creep, strain rate effects on strength, secondary consolidation, thixotropy, aging, pile capacity, and changes in penetration resistance (Mitchell 1960, Kulhawy and Mayne 1990, Mesri et al. 1990, Schmertmann 1991, Díaz-Rodríguez and Santamarina 1999).

The coexistence of multiple internal spatial and temporal scales in particle forces hints to important potential effects when trying to relate laboratory measurements to field parameters (strength, stiffness, diffusion and conduction parameters). Thus, parameters obtained in the lab must be carefully interpreted in order to select design parameters.

Reassessing Customary Concepts

Many commonly used concepts and accepted soil phenomena gain new clarity when they are re-interpreted at the level of particle forces. The principle of effective stress and the phenomenon of hydraulic fracture in soils are briefly addressed next.

Effective Stress and Modified Effective Stress Expressions

The concept of effective stress plays a pivotal role in understanding and characterizing soil behavior. Several earlier observations are relevant to the concept of effective stress, in particular:

- The hydrostatic pore pressure around a particle provides buoyancy. The intensity of the pore pressure around a particle does not affect the skeletal force transmitted between particles (Figure 4).
- Hydraulic gradients i cause fluid flow. The ensuing drag and velocity gradient forces act on particles and alter the effective stress transmitted by the skeleton.
- Changes in electrical and pendular capillary forces produce changes in volume, stiffness and strength, particularly in the finer soils and at low confinement (Figure 8).

Skeletal forces are defined at the boundaries (e.g., membrane in a triaxial specimen or equipotential lines in seepage) while other forces are determined at the particle or contact levels. Therefore the impact of these forces on soil behavior is different, and mixing both types of forces in a single algebraic expression can lead to incorrect predictions (as observed in Bishop and Blight 1963, for unsaturated soils). For example, some soils collapse upon wetting even though suction decreases and expansion should be expected; others experience a decrease in stiffness with an increase in ionic concentration even though a lower repulsion force is expected.

It follows from this discussion, that the use of modified effective stress expressions to accommodate suction or electrical repulsion and attraction forces should be discontinued (modified effective stress expressions are tabulated in Santamarina et al. 2001-a). Instead, behavior should be re-interpreted taking into consideration the separate and independent contributions of the skeletal force due to boundary loads and the other contact-level forces. This has been recognized in unsaturated media (Fredlund and Morgenstern 1977; Alonso et al. 1990), but it still

requires further attention in the context of contact-level electrical forces (developments in constitutive modeling can be found Gajo et al. 2001; Guimaraes et al. 2001; Frijns et al. 1997).

Hydraulic Fracture in Soils

Hydraulic fracturing is intentionally or unintentionally produced in soil masses in a wide range of situations: thermal changes (both in the laboratory and in in situ, such as in thermal ground improvement techniques - Figure 16-a), as an experimental tool to determine the state of stress (similar to applications in intact rocks – reviewed in Ladd et al. 1977), it has been hypothesized as a failure mechanism in the failure of large dams (including Teton dam – exacerbated by arching and stress redistribution), it has been used in the context of deformation control (Mair and Hight 1994; Jafari et al. 2001), it is routinely utilized to increase the hydraulic conductivity (in view of enhanced oil recovery or even in decontamination strategies), and it occurs during grouting (even when compaction grouting is intended).

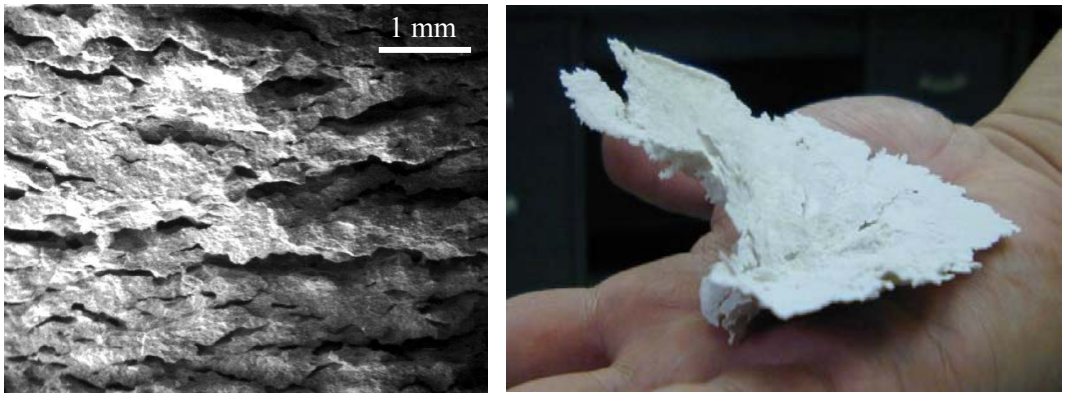

Figure 16. Hydraulic fracture in soils. It can take place in both fine grained soils (electrical attraction greater than particle weight) and in uncemented coarse grained soils (electrical attraction is irrelevant). (a) Kaolinite specimen mixed with water at the LL, and subjected to microwave radiation for fast heating. (b) Grouting in Ottawa sand: the picture shows the fracture that formed by grouting gypsum after the gypsum hardened and was retrieved - obtained in cooperation with L. Germanovich.

How can hydraulic fracture take place in soils? Current fracture mechanics theories apply to media with tensile strength and fracture propagation involves tensile failure at the tip. Yet, there is virtually no tensile capacity in uncemented soils. For clarity, consider uncemented dry sands where the adhesion force between particles is much smaller than the weight of particles (Figure 16-b; refer to Figure 8). The stress anisotropy in soils cannot exceed the limiting anisotropy determined by friction, say $\sigma_1/\sigma_3=\tan^2(45+\phi/2)$. Then, it appears that hydraulic fracturing in soils is the result of yield at the tip (stress path similar to AE), probably combined with other phenomena

such as hydrodynamic drag and/or cavitation of the pore fluid in the process zone. From this perspective, the application of standard fracture mechanics theory invoking the undrained shear strength of the soil as a form of cohesion violates the fundamental behavior of soils.

Closing remarks

Summary of Main Observations. Discerning soil behavior at the microscale brings enhanced physical meaning and understanding that can be applied to comprehend both available results and new measurements. Such insight guides research as well as the understanding of soil behavior in view of engineering applications. The main observations follow:

- Soils are particulate materials. Therefore, particle forces determine soil response. Particle forces are interrelated with particle characteristics (including size and distribution, slenderness, mineralogy), contact behavior and fabric .
- The behavior of coarse-grained soils is controlled by skeletal forces related to boundary stresses. On the other hand, the finer the particle and the lower the effective confinement, the higher the relevance of contact-level electrical and capillary forces. The transition size from coarse to fine for standard engineering applications is around $d \approx 10\mu m$.
- Hydrodynamic forces alter the skeletal forces and can displace movable particles. Either fines migration or clogging renders non-linear fluid flow, and affects the pore pressure distribution and the effective stress.
- Cementation, even if small, alters stiffness, strength and volume change tendencies. Two regions can be identified: the low-confinement cementation-controlled region and the high-confinement stress-controlled region.
- While previously suggested modified effective stress expressions can incorporate the various contact-level forces, they are physically incorrect and can lead to inadequate predictions. Therefore, their use should be discontinued.
- The drained strength of a soil reflects the balance between two competing micro-processes: the decrease in inter-particle coordination to reduce rotational frustration (in order to minimize friction), and the buckling of chains (that increases coordination).
- The undrained strength is determined by the (tendency to) volume compressibility of the skeleton, which depends on the vulnerability of load carrying chains.
- The degradation threshold strain in coarse soils increases with the applied load and decreases with the stiffness of the particles. In fine grain soils, it increases with the effective distance of electrical forces and with decreasing particle size, hence, the higher the plastic index the higher the degradation threshold strain.
- There are multiple internal scales inherent to particle forces in soils (both spatial and temporal).
- The re-interpretation of common concepts at the level of particle forces, such as "cohesive soil", "effective stress" and "hydraulic fracture", provides enhanced insight into soil behavior.

Current Capabilities. The soil researcher today has exceptional experimental and numerical tools to study soil behavior, including particle forces. Likewise, today's geotechnical engineer can use robust, versatile and inexpensive numerical capabilities, standard testing methods, and a new generation of testing principles and procedures. These tools must be implemented within the framework of a clear understanding of soil behavior.

Challenging future. There are abundant fascinating research questions in soil behavior, including: the implications of omnipresent strain-localization and multiple internal scales on soil properties and engineering design; the reinterpretation of friction in light of a large number of new studies (coarse and fine soils) and harnessing friction through inherent noise-friction interaction; new characterization-rehabilitation methodologies based on dynamic energy coupling; bio-geo phenomena; methane hydrates (characterization and production); and subsurface imaging (similar to medical diagnosis) combined with the determination of engineering design parameters or within the framework of an advanced observational approach.

Today's availability and easy access to information were unimaginable only 20 years ago. Yet, paradoxically, this great facility to access almost unlimited information appears to enhance the risk of forgetting knowledge. Indeed, we are challenged not only to address new fascinating questions, but also to preserve the great insight and understanding developed by the preceding generations. This should be our commitment today, as we celebrate Prof. C. Ladd's leading example.

Acknowledgements

Prof. Ladd's contributions have profoundly enhanced our understanding of soil behavior and its implementation in engineering design. Many colleagues provided valuable comments and suggestions, including: J. Alvarellos, S. Burns, G. Cascante, G.C. Cho, D. Fratta, D. Frost, L. Germanovich, M.S. Guimaraes, I. Herle, K.A. Klein, J.S. Lee, P. Mayne (his knowledge of the literature is enviable), A.M. Palomino, G. Rix, J.R. Valdes, V. Uchil (for the many runs to the library), Y.H. Wang, and exceptional anonymous reviewers. References acknowledge the insight gained from other authors. Funding was provided by the National Science Foundation.

References

Airey, D.W. and Fahey, M. (1991), Cyclic Response of Calcareous Soil from the North-West Shelf of Australia, Géotechnique, vol. 41, no. 1, pp. 101-121.

Alonso, E.E. Gens A. and Josa, A. (1990), A constitutive Model for Partially Saturated Soils, Géotechnique, vol. 40, no. 3, pp. 405-430.

Bear, J. (1972), Dynamics of Fluids in Porous Media, Dover, New York, 764 pages.

Bennett, R.H. and Hulbert, M.H. (1986), Clay Microstructure, International Human Resources Development Corporation, Boston, 161 pages.

Bhushan, B., Israelachvili, J. N. and Landman, U. (1995), Nanotribology: Friction, wear and lubrication at the atomic scale, Nature, vol. 374, pp. 607-616.

Bishop, A. W. and Blight, G. E. (1963), Some aspects of effective stress in saturated and partly saturated soils, Géotechnique, vol. 13, pp. 177-196.
Bishop, A.W. and Garga, V.K. (1969), Drained Tension Tests on London Clay, Géotechnique, vol. 19, pp. 309-313.
Bjerrum, L. (1972), Embankments on Soft ground, Proc. Earth & Earth-Supported Structures (Purdue Conference), vol. 2, ASCE, Reston, Virginia, pp 1-54.
Bolton, M. D. (1986), The strength and dilatancy of sands, Géotechnique, vol. 36, pp. 65-78.
Campanella R.G. and Vaid, Y.P. (1972), A simple Ko Triaxial Cell, Canadian Geotechnical Journal, vol. 9, pp.249-260.
Castro G. (1969), Liquefaction of Sands, Ph.D. Dissertation, Harvard University, Massachusetts, 112 pages.
Chantawarangul, K. (1993), Numerical Simulation of Three-Dimensional Granular Assemblies, Ph.D. Dissertation, University of Waterloo, Ontario, 219 pages.
Cho, G.C. and Santamarina, J.C. (2001), Unsaturated Particulate Materials - Particle Level Studies, ASCE Geotechnical Journal, vol. 127, no. 1, pp. 84-96.
Cho, G.C. (2001), Unsaturated Soil Stiffness and Post Liquefaction Shear Strength (Chapter III: Omnipresent Localizations), PhD Dissertation, Georgia Institute of Technology, 288 pages.
Clough, G.W., Sitar, N., Bachus, R.C. and Rad, N.S. (1981), Cemented Sands Under Static Loading. Journal of Geotechnical Engineering, ASCE, vol. 107, no. 6, pp. 799-817.
Cornforth, D.H. (1964), Some Experiments on the Influence of Strain Conditions on the Strength of Sand, Géotechnique, vol. 14, no. 2, pp. 143-167.
Cuccovillo, T. and Coop, M.R. (1997), Yielding and Pre-Failure Deformation of Structure Sands, Géotechnique, vol. 47, no. 3, pp. 491-508.
Cundall, P.A. and Strack, O.D.L. (1979), A discrete Numerical Model for Granular Assemblies, Geotechnique, vol. 29, no. 1, pp. 47-65.
Dantu, P. (1968), Etude Statistique des Forces Intergranulaires dans un Milieu Pulverulent, Géotechnique, vol. 18, pp. 50-55.
Delage, P. and Lefebvre, G. (1984), Study of the structure of a sensitive Champlain clay and of its evolution during consolidation, Canadian Geotechnical Journal, vol. 21, pp. 21-35.
Delville, A. (1995), Monte Carlo Simulations of Surface Hydration: An Application to Clay Wetting, J. Phys. Chem. vol. 99, pp. 2033-2037.
Delville, A. (2001), The Influence of Electrostatic Forces on the Stability and the Mechanical Properties of Clay Suspensions, Proc. Workshop on Clay Behaviour: Chemo-Mechanical Coupling, Edts., C. Di Maio, T. Hueckel, and B. Loret, Maratea, Italy. 20 pages.
Deresiewicz, H. (1973), Bodies in contact with applications to granular media, Mindlin and Applied Mechanics, Edited by B. Herrman, Pergamon Press, New York.
Desrues, J., Chambon, R., Mokni, M. and Mazerolle, F. (1996), Void Ratio Evolution Inside Shear Bands in Triaxial Sand Specimens Studied by Computed Tomography, Geotechnique, vol. 46, no. 3, pp. 529-546.

Díaz-Rodríguez, J.A. and Santamarina, J.C. (1999), Thixotropy: The Case of Mexico City Soils, XI Panamerican Conf. on Soil Mech. and Geotech. Eng., Iguazu Falls, Brazil, Vol. 1 pp. 441-448.

Drescher, A. and de Josselin de Jong, G. (1972), Photoelastic Verification of a Mechanical Model for the Flow of a Granular Material, J. Mechanics and Physics of Solids, vol. 20, pp. 337-351.

Duffy, J. and Mindlin, R. D. (1957), Stress-strain relations of a granular medium, Journal of Applied Mechanics, vol. 24, pp. 585-593.

Durelli, A. J. and Wu, D. (1984), Loads between disks in a system of discrete elements, Experimental Mechanics, December, pp. 337-341.

Emerson, W.W. (1959), The structure of Soil Crumbs, J. Soil Science, vol. 10, no. 2, pp. 234.

Fernandez, A. and Santamarina, J.C. (2001), The Effect of Cementation on the Small Strain Parameters of Sands, Canadian Geotechnical Journal, vol. 38, no. 1, pp. 191-199.

Finno, R.J., Harris W.W., Mooney, M.A. and Viggiani, G. (1997), Shear Bands in Plane Strain Compression of Loose Sand, Géotechnique, vol. 47, no. 1, pp. 149-165.

Fredlund, D. G. and Morgenstern, N. R. (1977), Stress state variables for unsaturated soils, Journal of Geotechnical Engineering, ASCE, vol. 103, pp. 447-466.

Fredlund, D. G., and Rahardjo, H. (1993). Soil Mechanics for Saturated Soils. John Wiley and Sons, New York.

Frijns, A.J.H., Huyghe, J.M. and Janssen, J.D. (1997), A Validation of the Quadriphasic Mixture Theory for Intervertebral Disc Tissue, Int. Journal Engineering Science, vol. 35, pp. 1419-1429.

Gajo, A., Loret, B. and Hueckel, T. (2001), Electro-Chemo-Mechanical Coupling in Homoionic and Heteroionic Elastic-Plastic Expansive Clays, Proc. Workshop on Clay Behaviour: Chemo-Mechanical Coupling, Edts., C. Di Maio, T. Hueckel, and B. Loret, Maratea, Italy. 26 pages.

Gherbi, M. Gourves, R. and Oudjehane, F. (1993), Distribution of the Contact Forces Inside a Granular Material, Powders and Grains 93, Prod. 2nd International Conference on Micromechanics of Granular Media, Brimingham, Elsevier, Amsterdam, pp. 167-171.

Graf, W.H. (1984), Hydraulics of Sediment Transport, Water Resources Publications, Highlands Ranch, Colorado, 513 pages.

Guimaraes, L., Gens, A, Sanchez, M. and Olivella, S. (2001), A Chemo-Mechanical Model for Unsaturated Expansive Clays, Proc. Workshop on Clay Behaviour: Chemo-Mechanical Coupling, Edts., C. Di Maio, T. Hueckel, and B. Loret, Maratea, Italy. 28 pages.

Hanzawa, H. (1980), Undrained Strength and Stability Analysis for a Quick Sand, Soils and Foundations, vol. 20, no. 2, pp. 17-29.

Horn, R.G. and Israelachvili, J. (1981), Direct Measurement of Structural Forces Between Two Surfaces in a Non-Polar Liquid, J. Chemical Physics, vol. 75, no. 3, pp. 1400-1411.

Ingles, O.G. (1962), Bonding Forces in Soils - Part 3, Proc. Of the First Conference of the Australian Road Research Board, vol. 1, pp. 1025-1047.

Ishihara, K. (1996), Soil Behaviour in Earthquake Geotechnics, Calderon Press, Oxford, 350 pages.
Israelachvili, J. (1992), Intermolecular and Surface Forces, Academic Press, New York, 450 pages.
Jafari, M.R., Au, S.K., Soga, K., Bolton, M.D. and Komiya, K. (2001), Fundamental Laboratory Investigation of Compensation Grouting in Clay, Cambridge University, 15 pages.
Jaeger, H. M., Nagel, S. R. and Behringer, R. (1996), The physics of granular materials, Physics Today, April, pp. 32-38.
Jamiolkowski, M., Ladd, C.C., Germaine, J.T. and Lancellotta, R. (1985), New Developments in Field and Laboratory Testing of Soils, Proc. 11th ICSMFE, San Francisco, vol. 1, pp 67-153.
Jang, D.J. and Frost, J.D. (1998), Sand Structure Differences Resulting from Specimen Preparation Procedures, Prod. ASCE Conf. Geotechnical Earthquake Engineering and Soil Dynamics, Seattle, vol. 1, pp. 234-245.
Kulhawy, F.H. and Mayne, P.W. (1990), Manual on Estimating Soil Properties for Foundation Design, EPRI EL-6800, Electric Power Research Institute, Palo Alto.
Kuhn, M. R. and Mitchell, J.K. (1993), New Perspectives on Soil Creep, ASCE J. Geotechnical Engineering, 119(3): 507-524.
Ladd, C.C. (1959), Mechanisms of Swelling by Compacted Clays, Highway Research Board Bulletin 245, pp. 10-26.
Ladd, C.C. and Lambe, T.W. (1963), The strength of Undisturbed Clay Determined from Undrained Tests, NRC-ASTM Symposium on Laboratory Shear Testing of Soils, Ottawa, ASTM STP 361, pp. 342-371.
Ladd, C.C. (1967), Discussion, Proc. Geotechnical Conference on Shear Strength Properties of Natural Soils and Rocks, NGI, Oslo, vol. 2, pp. 112-115.
Ladd, C.C., Foott, R., Ishihara, K., Schlosser, F. and Poulos, H.G. (1977), Stress-Deformation and Strength, Proc. 9th ICSMFE, vol. 2, Tokyo, pp. 421-494.
Ladd, C.C. (1991), Stability Evaluation during Staged Construction, J. Geotechnical Engineering, vol. 117, no. 4, pp. 540-615.
Lade, P.V. and Duncan, J.M. (1975), Elasto-plastic Stress-Strain Theory for Cohesionless Soil, ASCE Journal of Geotechnical Engineering, vol. 101, no. 10, pp. 1037-1053.
Lade, P.V. and Overton, D. D. (1989), Cementation effects in Frictional Materials, ASCE Journal of Geotechnical Engineering. 115, pp. 1373-1387.
Landman, U., Luedtke, W.D. and Gao, J.P. (1996), Atomic-Scale Issues in Tribology: Interfacial Junctions and Nano-Elastohydrodynamics. Langmuir, vol. 12, pp. 4514-4528.
Lanier, J., Viggiani, G. and Desrues, J. (1997), Discussion to the paper by J. Chu, R. Lo and I.K.Lee entitled Strain Softening and Shear band Formation of Sand in Multi-axial Testing, Geotechnique, vol. 47, no. 5 pp. 1073-1077.
Larsen, G. and Chilingar, G.V. (1979), Diagenesis in Sediments and Sedimentary Rocks, Elsevier Scientific Publishing Company, New York, N.Y.
Leroueil, M.S. (2001) Natural Slopes and Cuts: Movement and Failure Mechanisms, Géotechnique, vol. 51, no. 3, pp. 195-244

Mair, R.J. and Hight, D.W. (1994), Compensation Grouting, World Tunneling, November, pp. 361-367.
Mayne, P.W. and Holtz, R.D. (1985), Effect of principal stress rotation on clay strength, Proc. 11th ICSMFE, San Francisco, vol. 2, pp 579-582.
Mesri, G., Feng, T.W. and Benak, J.M. (1990), Postdensification Penetration Resistance of Clean Sands, vol. 116, no. 7, pp. 1095-1115.
Mitchell, J.K. (1993), Fundamentals of Soil Behavior, J.Wiley, New York, 437 pages.
Mitchell, J.K. (1960), Fundamentals Aspects of Thixotropy in Soils, Journal of the Soil Mechanics and Foundations Division, ASCE, vol. 86, no. 3, pp. 19-52.
Mokni, M. and Desrues, J. (1998), Strain Localization Measurements in Undrained Plane-Strain Biaxial Tests on Hostun RF Sand, Mechanics of Cohesive-Frictional Materials, vol. 4, pp. 419-441.
Muhunthan, B. (1991), Liquid Limit and Surface Area of Clays, Géotechnique, vol. 41, pp. 135-138.
Öberg, A.L. (1997), Matrix Suction in Silt and Sand Slopes, Ph.D. Dissertation, Chalmers University of Technology, Sweden, 160 pages.
Oda, M., Nemat-Nasser, S. and Konishi, J. (1985), Stress-Induced Anisotropy in Granular Masses, Soil and Foundation, vol. 25, pp. 85-97.
Oda, M. (1972), The mechanism of fabric changes during compressional deformation of sand, Soils and Foundations, vol. 12, no. 2, pp. 1-18.
Oda, M. and Kazama, H. (1998), Microstructure of Shear Bands and its Relation to the Mechanism of Dilatancy and Failure of Dense Granular Soils, Géotechnique, vol. 48, no. 4, pp. 465-481.
Parry, R.H.G. (1960), Triaxial Compression and Extension Tests on Remoulded Saturated Clay, Géotechnique, vol. 10, pp. 166-180.
Persson, B. N. J. (1998), Sliding Friction - Physical Principles and Applications, Springer, New York, 462p.
Radjai, F., Wolf, D.E., Jean, M. and Moreau, J.J. (1998), Bimodal Character of Stress Transmission in Granular Packings, Physical review Letters, vol. 80., no. 1, pp. 61-64.
Reddy, K.R. and Saxena, S.K. (1993), Effects of Cementation on Stress-Strain and Strength Characteristics of Sands, Soils and Foundations, vol. 33, no. 4, pp. 121-134.
Rinaldi, V.A. (1998), Changes in electrical conductivity after remolding a clayey soil, personal communication. A similar effect was observed in Mexico City soils and is documented in Diaz-Rodriguez and Santamarina, 1999.
Robertson, P.K. et al. (2000), The CANLEX Project: Summary and Conclusions, Can. Geotechnical J., vol. 37, pp. 563-591.
Rothenburg, L. (1993), Effects of particle shape and creep in contacts on micromechanical behavior of simulated sintered granular media, Mechanics of Granular Materials and Powder Systems, vol. 37, pp. 133-142.
Rothenburg, L. and Bathurst, R. J. (1989), Analytical study of induced anisotropy in idealized granular material, Géotechnique, vol. 49, pp. 601-614.
Saada, A.S., Liang, L., Figueroa, J.L. and Cope, C.T. (1999), Bifurcation and Shar Band Propagation in Sands, Géotechnique, vol. 49, no. 3, pp. 367-385.
Santamarina, J.C., Klein, K. and Fam, M. (2001-a), Soils and Waves, J. Wiley, Chichester, UK, 488 pages.

Santamarina, J.C, Klein, K. Palomino, A. and Guimaraes, M (2001-b), Micro-Scale Aspects Of Chemical-Mechanical Coupling - Interparticle Forces And Fabric; Edts., C. Di Maio, T. Hueckel, and B. Loret, Maratea, Italy. 26 pages.

Santamarina, J.C. (1997), 'Cohesive Soil:' A Dangerous Oxymoron, The Electronic J. Geotechnical Eng. - Magazine, August (URL: under Electronic Publications in http://www.ce.gatech.edu/~carlos).

Schanz, T. and Vermeer, P.A. (1996), Angles of friction and dilatancy in sand, Géotechnique, vol. 46, no. 1 , pp. 145-151.

Schmertmann, J.H. (1991), The Mechanical Aging of Soils, ASCE J. Geotechnical Engineering, vol. 117, no. 9, pp.1288-1330.

Schofield, A. (1998), Don't Use the C-Word, Ground Engineering, August, pp. 29-32.

Skipper, N.T. (2001), Influence of Pore-Liquid Composition on Clay Behaviour: Molecular Dynamics Simulations of Nano-Structure, Proc. Workshop on Clay Behaviour: Chemo-Mechanical Coupling, Edts., C. Di Maio, T. Hueckel, and B. Loret, Maratea, Italy. 18 pages.

Skipper, N.T., Refson, K. and McConnell, J.D.C. (1991), Computer Simulation of Interlayer Water in 2:1 Clays, J. Chemical Physics 94, no. 11, pp. 7434-7445.

Sridharan, A., Altschaeffle, A. G. and Diamond, S. (1971), Pore size distribution studies, Journal of the Soil Mechanics and Foundations Division, Proceedings of the ASCE, vol. 97, SM 5, pp. 771-787.

Stokoe, K.H. and J.C. Santamarina (2000), Seismic-Wave-Based Testing in Geotechnical Engineering, GeoEng 2000, Melbourne, Australia, November, pp. 1490-1536

Tatsuoka, F. and Shibuya, S. (1992), Deformation Characteristics of Soils and Rocks from Field and laboratory Tests, The University of Tokyo, vol. 37, no. 1, 136 pages.

Terzaghi, K (1920), Old Earth Pressure Theories and New Test Results, Engineering News-Record, vol. 85, n. 14, pp. 632-637.

Thornton, C. (2000), Numerical Simulations of Deviatoric Shear Deformation of Granular Media, Geotechnique, vol. 50, pp. 43-53.

Vaid, Y.P. and Sayao, A. (1995), Proportional Loading Behavior in Sand Under Multiaxial Stresses, Soils and Foundations, vol. 35, no.3, pp. 23-29.

Vaid, Y.P. and Sivathayalan, S. (1996), Static and Cyclic Liquefaction Potential of Fraser Delta Sand in Simple Shear and Triaxial Tests, Canadian Geotechnical J., vol. 33, pp. 281-289.

Vaid, Y.P. and Sivathayalan, S. (2000), Fundamental Factors Affecting Liquefaction Susceptibility of Sands, Can. Geotechnical J., vol. 37, pp. 592-606.

Valdes, J.R. (2002), Fines Migration and Formation Damage, PhD Dissertation, Georgia Institute of Technology.

van Olphen, H. (1991), An Introduction to Clay Colloid Chemistry, Krieger Publishing Cy, Florida, pp. 318.

Vardoulakis, I. (1996), Deformation of Water-Saturated Sand: I. Uniform Undrained Deformation and Shear Banding, Géotechnique, vol. 46, no. 3, pp. 441-456.

Vucetic, M. and Dobry, R. (1991), Effect of soil plasticity on cyclic response, Journal of Geotechnical Engineering, ASCE, vol. 117, pp. 89-107.

Wang, Q. and Lade, P.V. (2001), Shear Banding in True Triaxial Tests and Its Effect on Failure of Sand, in print.

Yoshimine, M., Robertson, P.K. and Wride, C.E. (1999), Undrained Shear Strength of Clean Sands to Trigger Flow Liquefaction, Canadian Geotechnical Journal, vol. 36, pp. 891-906.

Zdravkovic, L. and Jardine, R.J. (1997), Some Anisotropic Stiffness Characteristics of a Silt Under General Stress Conditions, Géotechnique, vol. 47, no. 3, pp. 407-437.